RSC Advances

PAPER

View Article Online
View Journal | View Issue

Cite this: *RSC Adv.*, 2017, **7**, 38187

Facile fabrication of flexible core–shell graphene/conducting polymer microfibers for fibriform supercapacitors†

Yuning Meng,[ab] Lin Jin,[*a] Bin Cai[b] and Zhenling Wang[*a]

The doping method is typically applied to highly flexible graphene fibers to improve their gravimetric energy storage capacity and electrical conductivity. However, the applications of these graphene fibers, used for flexible wearable supercapacitors, are limited because of their poor mechanical performance and uniform phase. We fabricated graphene core, conductive polymer (PEDOT) shell fibers (GF@PEDOT) using a hydrothermal strategy combined with an *in situ* interfacial polymerization method. The unique cloth-like structure granted the graphene fibers excellent electrochemical performance and greatly enhanced their flexibility. Furthermore, the prepared symmetric fiber supercapacitors based on two intertwined GF@PEDOT electrodes with a poly(vinyl alcohol) PVA/H_2SO_4 gel electrolyte exhibited high flexibility with a specific capacitance of up to 15.39 mF cm^{-2} (0.58 mF cm^{-1}) at 0.53 mA cm^{-2}. Combined with the excellent integrated performance, we anticipate this type of core–shell fiber supercapacitors to have promising applications in the next generation of wearable electronics and as highly stretchable supercapacitors.

Received 14th June 2017
Accepted 21st July 2017

DOI: 10.1039/c7ra06641d

rsc.li/rsc-advances

1. Introduction

Flexible, wearable energy storage and conversion devices are flourishing due to their compatibility with the miniaturization and integration of multiple electronic devices.[1–10] Supercapacitors (SCs) are one type of energy storage devices that possess a high power density, a fast charge/discharge rate and long cycling life and have been widely used in hybrid electric vehicles, energy management, memory back-up devices and industrial power.[11–15] Graphene fibers (GFs), a type of macroscopic, one-dimensional material, assembled into graphene sheets have emerged in the development of flexible wearable electronic devices because of their light weight, mechanical flexibility for textiles and ease of functionalization.[16–18] SCs based on GF, which combine the advantages of GF and SCs, have been widely investigated.[19–26] However, compared to traditional planar supercapacitors, SCs based on GF show much lower energy densities and specific capacitance due to lower exposed surface areas; on the other hand, the traditional supercapacitors suffer from a great challenge in mechanical performance. Therefore, researchers are attracted to exploring fiber supercapacitors with both high specific capacitance and good mechanical properties. In our previous study, we fabricated the all-graphene core–sheath fiber; a core of GF is covered with a sheath of 3D, porous, network-like graphene framework. The assembled fiber supercapacitor, using a gel electrolyte, is highly flexible due to this hierarchical hybrid structure, and can be used for spring supercapacitors with high compressibility and stretchability. However, the measured area-normalized capacitance was only 1.2–1.7 mF cm^{-2}.[19] In order to solve this problem, we deposited MnO_2 nanostructures on the 3D graphene framework, causing the areal capacitance to increase to 9.1–9.6 mF cm^{-2}.[22] Nevertheless, the specific capacitance, conductivity and mechanical properties of SCs based on GF should be further improved.

Poly(3,4-ethylenedioxythiophene) (PEDOT), as a polythiophene derivative, is well known to be useful as the active material for supercapacitor electrodes because of its high conductivity, thermal stability, good mechanical strength and high stability even in the oxidized state.[27,28] Furthermore, PEDOT can charge both Faradaically and non-Faradaically, and can be conveniently deposited.[27] Nowadays, PEDOT has been processed into various macroscopic architectures, for example transparent, conductive films and 3D frameworks, which have been fabricated for various applications from energy to the biomedical field.[29–34]

In this study, we use a facile yet efficient strategy to fabricate one-dimensional, conductive polymer coated GF shell–core structured GF-PEDOT fibers. First, we fabricated GFs by a facile, one-step, dimensionally-confined hydrothermal strategy;

[a]*The Key Laboratory of Rare Earth Functional Materials and Applications, Zhoukou Normal University, Zhoukou 466001, P. R. China. E-mail: jinlin_1982@126.com; zlwang2007@hotmail.com; Fax: +86-394-8178518; Tel: +86-394-8178518*

[b]*School of Chemistry and Chemical Engineering, Zhoukou Normal University, Zhoukou 466001, P. R. China*

† Electronic supplementary information (ESI) available. See DOI: 10.1039/c7ra06641d

second, PEDOT was coated on the surface of GFs by using the *in situ* interfacial polymerization method. This core–shell structure fiber is denoted as GF@PEDOT, which has high flexibility and electrical conductivity. Moreover, they can be tied into knots and woven into cloth-like structures by hand, thus offering potential electrodes for wearable electronics. Symmetric fibriform supercapacitors based on two intertwined GF@PEDOT electrodes and poly(vinyl alcohol) PVA/H_2SO_4 gel electrolyte showed high flexibility and specific capacitance. The GF@PEDOT fiber supercapacitors demonstrate specific areal capacitances up to 15.39 mF cm^{-2} (or 0.58 mF cm^{-1}) at 0.53 mA cm^{-2}.

2. Experimental

2.1 Materials

Graphene oxide (GO) powder was purchased from Nanfeng Co., Jiangsu. Moreover, 3,4-ethylenedioxythiophene (EDOT) (98%), $FeCl_3$ (98%), $LiClO_4$ (98%), poly(vinyl alcohol) PVA ($M = 1750 \pm 50$), absolute ethanol and concentrated H_2SO_4 were obtained from Sigma-Aldrich. All chemicals were used as received without further purification.

2.2 Preparation of GF@PEDOT

GO solution at a concentration of 8 mg mL^{-1}, prepared using ultrasonication, was injected into a glass pipeline at a slow rate and baked in an oven at 230 °C for 2 h, after sealing the two ends of the pipeline. Graphene fiber was released from the pipeline by the flow of air and then was held on glass slides for drying in air. Graphene fibers were prepared as mentioned our previous study.[17] Subsequently, the GFs were immersed into a solution of EDOT–$FeCl_3$ in ethanol (EDOT: 0.05 g mL^{-1}, $FeCl_3$: 0.05 g mL^{-1}) for 30 s at room temperature. As the ethanol evaporated, the polymerization of EDOT started, forming a PEDOT shell on the surface of the GFs. The obtained GF@PEDOT fibers were washed several times using deionized water to remove residual reagents completely. Finally, the sample was dried in air for 30 min.

2.3 Preparation of GF@PEDOT fiber SC

First, a PVA/H_2SO_4 gel electrolyte was prepared as follows: 1 g concentrated sulfuric acid was mixed with 10 mL deionized water and 1 g PVA ($M = 1750 \pm 50$) powder was added. The entire mixture was heated steadily to ~85 °C under vigorous stirring until the solution became clear. Then, the solution was kept at 85 °C without stirring.

Second, we intertwined two GF@PEDOT electrodes pre-coated with PVA/H_2SO_4 gel electrolyte to form the GF@PEDOT fiber SC.

2.4 Structural and chemical characterization

The morphology of the GF@PEDOT, graphene fibers and fiber supercapacitors were examined using a scanning electron microscope (SEM, Hitachi S-3000N) at an acceleration voltage of 10 kV. Infrared spectra were recorded on a Smart Omni-Transmission spectrometer with the solid sample compressed on a diamond plate. All samples and KBr were dried using an infrared lamp. Raman spectra were measured using a LabRAM HR Evolution (HORIBA Jobin Yvon, France) with an Ar laser at a wavelength of 532 nm. The mechanical properties were tested using an Instron material testing system (Instron 3342) with a preload of 0.5 N and strain rate of 1 mm min^{-1}.

2.5 Electrochemical investigation

All of the electrochemical curves (CV and galvanostatic charge–discharge) were obtained with an Autolab Pgstat 302N.

First, the cyclic voltammetry (CV) response of the GFs and GF@PEDOT was investigated in a three-electrode system. In this system, 1 M $LiClO_4$ aqueous solution was used as the electrolyte and Pt wire and Ag/AgCl (3 M KCl) were used as the counter and reference electrodes, respectively. GF@PEDOT and GF acted as the working electrodes. Second, we tested the GF@PEDOT fiber SC using CV and galvanostatic charge–discharge measurements in a two-electrode system. Finally, we investigated the fiber SC's electrochemical stability at different bending angles and its tolerance to repeated straightening-to-bending cycles in a two-electrode system.

3. Results and discussion

The preparation process of GF@PEDOT is schematically shown in Fig. 1a. GFs were fabricated by a facile yet efficient, one-step, dimensionally-confined, hydrothermal strategy from aqueous suspensions (detailed information can be found in the Experimental section).[17] Subsequently, PEDOT was coated onto the surface of the GF fibers *via in situ* interfacial polymerization using $FeCl_3$ as an oxidant.[28] Briefly, the GF fibers were immersed into the solution of EDOT–$FeCl_3$ in ethanol for 30 s at room temperature. As the ethanol evaporated, the polymerization of EDOT began, forming a PEDOT shell layer on the surface of the GFs. After 24 h of reaction, GF@PEDOT was obtained (photographs of the fabrication process are shown in Fig. S1†). These GF@PEDOT fibers were flexible enough to be intertwined or bent and woven into a cloth-like structure (Fig. 1b and c).

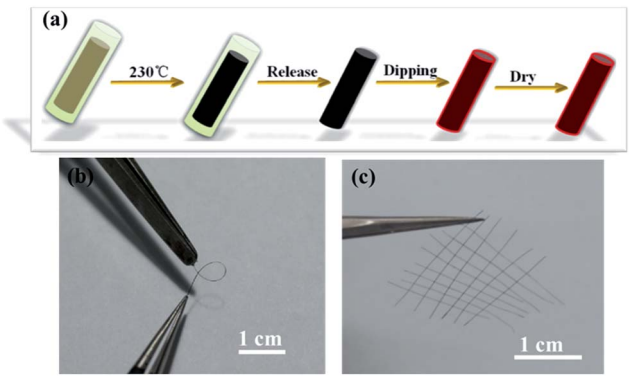

Fig. 1 (a) Schematic of GF@PEDOT fabrication. (b) Photograph of a GF@PEDOT in a bent state. (c) Photograph of the hand-knitted textile of GF@PEDOT fibers.

The GF@PEDOT fibers were analyzed *via* scanning electron microscopy (SEM). The surface of the GF was rough and wrinkled, and the GF had a diameter of 35 μm (Fig. S2a and b†), which offered a large area for interaction with PEDOT. After coating with PEDOT, the diameter significantly increased to a value of up to 90 μm. Moreover, its surface was uniform, which has advantages for electron transportation (Fig. 2a and b). The cross-section views (Fig. 2c and d) clearly show that the core–shell structure was present and that the shell PEDOT is in tight contact with the core GF, which also provides the mechanical stability of GF@PEDOT under deformation. The core–shell structure has a relatively higher tensile strength than that of the initial GF (Fig. S3†). It is very difficult to damage unless it receives a large mechanical external force (Fig. S2f†).

EDS mapping of sulfur shows that the PEDOT is uniformly distribute on the surface of the GF (Fig. S4a and e†). The chlorine, shown in Fig. S4b,† is from the residual oxidant $FeCl_3$. In addition, EDS mapping of GF@PEDOT indicated that C and O were present (Fig. S4c and d,† respectively).

Infrared spectra were recorded on a Smart Omni-Transmission spectrometer from solid sample compressed on a diamond plate. As EDOT started to polymerize, the characteristic peaks of PEDOT started to grow in the FT-IR spectra (Fig. S5a†), which include the symmetric and asymmetric C–O–C stretching at 1213 and 1116 cm^{-1}; the C=C stretching in the thiophene ring at 1445 cm^{-1}; the C–S characteristic absorption peaks at 986, 850 and 690 cm^{-1}. The peak at 1627 cm^{-1} is from the C=C skeleton stretching in the GFs. Fig. S5b† shows typical Raman spectrum ($\lambda = 532$ nm) of GFs and GF@PEDOT. Moreover, 1349 and 1593 cm^{-1} are the D and G peaks of GF. The data from GF@PEDOT are in good agreement with previous experimental and theoretical studies of PEDOT.[23–39] The experimental frequencies of the PEDOT are shown in Table S1† compared with references. These results sufficiently demonstrate the successful polymerization of EDOT to form a PEDOT shell on the surface of GF.

In order to investigate the electrochemical performance of GF@PEDOT and pure GF, we first tested their cyclic voltammetry (CV) response in a three-electrode electrochemical cell. As shown in Fig. 3b, the CV curves of GF@PEDOT show ideal capacitive behavior with a nearly rectangular shape without apparent distortion under scan rate from 30 mV s^{-1} to 200 mV s^{-1}. This may result from the conductive shell of PEDOT, which is accessible for fast ion transportation, and the high capacitive behavior of the core GF.

Compared with GF@PEDOT, the CV curves for the pure GF present a shuttle-like shape with different scan rates (Fig. 3c), which may be caused by the compact structure of GF. Moreover, at the same voltage, the current value of GF@PEDOT (Fig. 3b) is up to 80 μA, which is almost three times the 30 μA of GF (Fig. 3c). In addition, at the scan rate of 10 mV s^{-1} CV curves (Fig. 3a) also clearly revealed that GF@PEDOT has more rapid charge transport and higher rate performance compared with GF.

As GF@PEDOT has high flexibility and capacitive behavior, we fabricated symmetric solid-state fiber supercapacitors based on GF@PEDOT electrodes using the PVA/H_2SO_4 gel electrolyte. Briefly, we intertwined two GF@PEDOT electrodes with PVA/H_2SO_4 gel electrolyte (Fig. 4a and b). The results show that the assembled fiber supercapacitor is flexible and mechanically stable, properties which are inherited from GF@PEDOT in combination with the polyelectrolyte (Fig. 4c). Conventional liquid electrolytes have various drawbacks, such as difficulty in device integration, leakage of electrolyte and environmental instability. In contrast, gel electrolytes not only overcome those drawbacks but also act as an effective separator to prevent the undesirable short circuit of two electrodes. The intertwining structure of two GF@PEDOT electrodes covered with H_2SO_4/PVA gel electrolyte is shown in Fig. 4d and e, indicating that the surface of GF@PEDOT is smooth due to the uniform coating of electrolyte gel, which can ensure an effective ion diffusion process for capacitor applications. At the same time, the figures

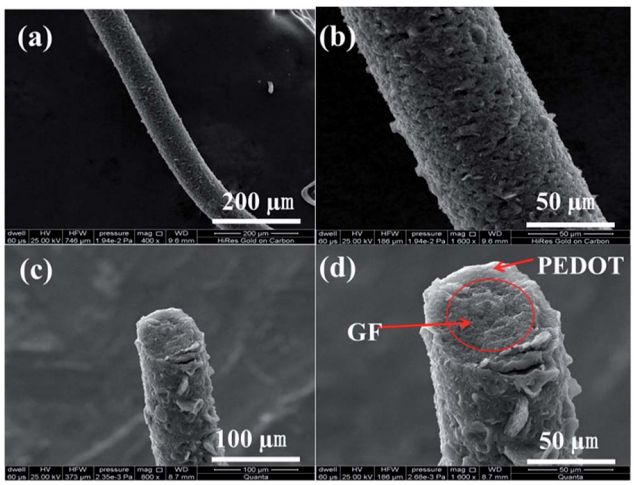

Fig. 2 (a, b) SEM images of a GF@PEDOT at different scales. (c, d) SEM images of the cross-section view showing the core–shell structure.

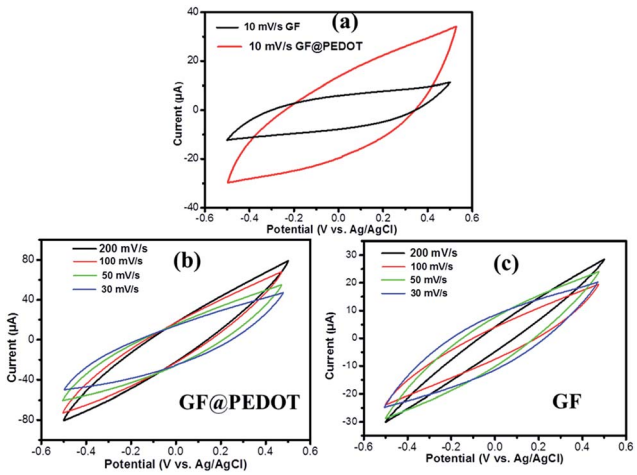

Fig. 3 (a) CV curves of GF@PEDOT and GF (the lengths of the samples were 1.5 cm) in 1 M $LiClO_4$ aqueous solution at 10 mV s^{-1}, (b) CV curves of GF@PEDOT and (c) GF at various scan rates.

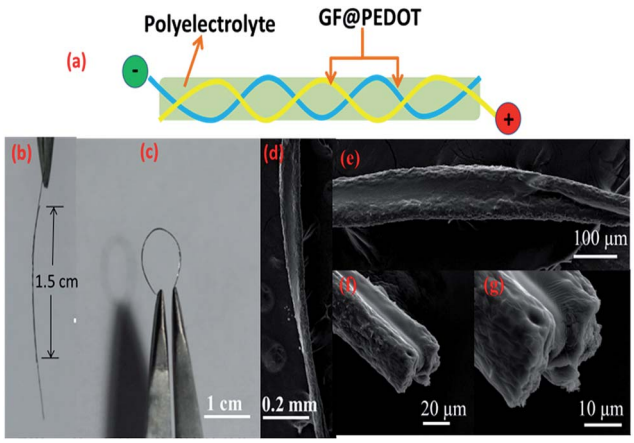

Fig. 4 (a) Schematic of fiber supercapacitor based on GF@PEDOT electrodes. (b) Photograph of a fiber supercapacitor whose active length is 1.5 cm. (c) Photograph of a fiber supercapacitor in a bent state. (d, e, f, g) SEM images of a fiber supercapacitor formed by intertwining two GF@PEDOT electrodes with polyelectrolyte (d, e) and its cross-section view (f, g).

clearly show that the gel electrolyte effectively separates the two electrodes to avoid short circuits. Fig. 4f is a cross-section view of a broken supercapacitor, revealing that the polyelectrolyte has fully permeated into the two GF@PEDOT electrodes and separated them (Fig. 4g is an enlarged view of Fig. 4f).

To investigate the electrochemical properties of the fiber supercapacitors, we characterized them using CV and galvanostatic charge–discharge measurements. CV curves of the symmetric solid-state fiber supercapacitors based on two GF@PEDOT electrodes and PVA/H_2SO_4 gel electrolyte with increasing scan rates from 30 mV s^{-1} to 120 mV s^{-1} are shown in Fig. 5a. The CV curves display a rectangular shape, which indicates the formation of an efficient electrochemical double layer capacitor with good charge propagation between the

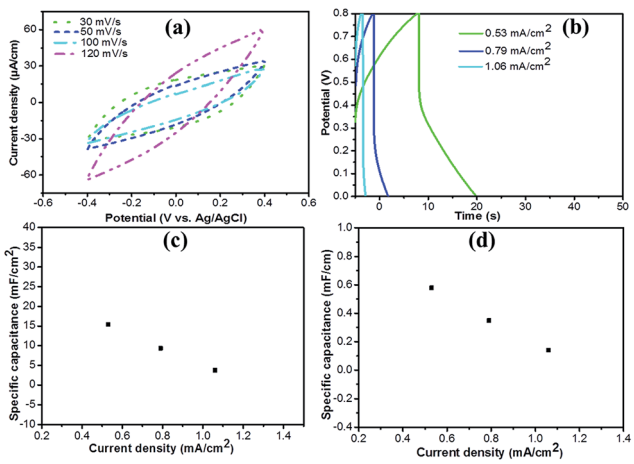

Fig. 5 (a) Cyclic voltammetry (CV) response and (b) galvanostatic charge–discharge profiles of the GF@PEDOT supercapacitor. (c) Area-specific capacitance and (d) length-specific capacitance of GF@PEDOT supercapacitor at different current density.

electrodes. Although the CV curves were slightly deformed with increasing scan rates, better capacitive behavior and higher current densities were observed in comparison with previous reports of supercapacitors based on GFs.[19]

Considering the special one-dimensional fiber configuration, the fiber supercapacitor mass is typically low; hence, the specific capacitance based on area and length is more useful for comparisons.[40] Fig. 5b shows the galvanostatic charge–discharge profiles for the fiber supercapacitor at current densities of 0.53 mA cm^{-2}, 0.79 mA cm^{-2} and 1.06 mA cm^{-2}. Although, it does not have a typical triangular shape or an evident voltage drop, the fiber supercapacitor has a specific areal capacitance of 15.39 mF cm^{-2} at 0.53 mA cm^{-2}, discounting the voltage drop. The calculated area-specific capacitance is 3.75–15.39 mF cm^{-2} (Fig. 5c), which exceeds that of all-graphene core–sheath fiber supercapacitors (1.2–1.7 mF cm^{-2}) and all-solid-state flexible supercapacitors based on a MnO_2/G/GF hybrid fiber (9.1–9.6 mF cm^{-2}).[19,22] Fig. 5d shows that the length-specific capacitance is about 0.14–0.58 mF cm^{-1}, which is almost 10 times that of all-graphene core–sheath fiber supercapacitors (20 μF cm^{-1}) and comparable to that of MnO_2/G/GF hybrid fiber supercapacitors (143 μF cm^{-1}).[19,22] The specific capacitance for the GF@PEDOT supercapacitor rapidly decreases with increasing current density as shown by the two curves in Fig. 5c and d. This phenomenon could be attributed to the shell PEDOT layer not fully showing its performance at high current densities. The energy density and power density of the GF@PEDOT supercapacitor are 0.117–3.95 × 10^{-7} W h cm^{-2} and 7.96–11.4 × 10^{-5} W cm^{-2} (Fig. S6†), respectively, which are comparable to that of all-graphene core–sheath fiber supercapacitors (energy density: 0.4–1.7 × 10^{-7} W h cm^{-2}, power density: 6–100 × 10^{-6} W cm^{-2}).[19] The energy density of GF@PEDOT supercapacitor is slightly lower than that reported for hollow graphene/conducting polymer fiber supercapacitors (energy density: 6.8 μW h cm^{-2}).[25]

To investigate the flexibility of the assembled fiber supercapacitor, we tested its specific capacitance during a long-term and repeated straight-to-bending process as described in Fig. 6a. The bending test of the fiber capacitor was carried out in a moving stage as schematically shown in Fig. S7a.† Fig. 6b shows that the CV curves kept a rectangular shape during the straight-to-bending process. As shown in Fig. 6c and d, the specific capacitance of the fiber SC remained at 0.45–0.55 mF cm^{-1} whether in the bending or straight state during 300 cycles, which indicates the excellent stability of the fiber SC under deformation. We also attempted to investigate how the bending angle influenced the capacitance of the fiber SC. Fig. S8† shows that at different bending angles, the specific capacitance of the fiber SC dropped only slightly. To further demonstrate the specific application of the fiber SC in wearable electronics, we implanted the fiber SC into a textile by hand weaving (Fig. S9a†). Fig. S9b† shows that the fiber SC maintains flexibility without the loss of capacitive performance after repeated bending. This indicates that the fiber SC could be used in the preparation of wearable or highly flexible electronics for energy storage.

We calculated the specific capacitance, energy density and power density of the GF@PEDOT supercapacitor on the basis of

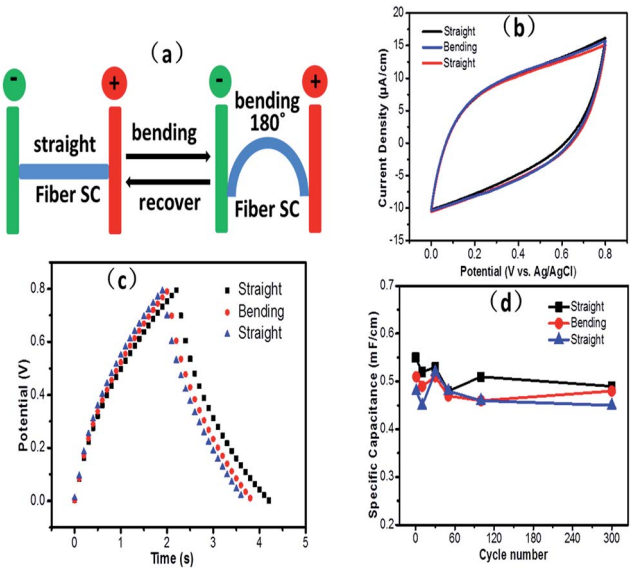

Fig. 6 (a) Schematic of a bending test. (b, c) CV and charge–discharge curves of a 1.5 cm fiber SC in straight and bending states (bending angle of ~180°) states, respectively. The scan rate in (b) is 10 mV s^{-1}. The current density in (c) is 1.56 mA cm^{-2}. (d) The capacitance stability of the fiber SC in bending and straight states undergoing 300 straight-bending cycles.

the galvanostatic charge–discharge curves. Specific measures were as follows:[19,41]

$$C = I/(\mathrm{d}V/\mathrm{d}t) \quad (1)$$

where C, I and $\mathrm{d}V/\mathrm{d}t$ are the capacitance, discharge current and the slope of the discharge curve, respectively.

$$C_{\mathrm{A}} = C/A \quad (2)$$

$$C_{\mathrm{L}} = C/L \quad (3)$$

where C_{A} and C_{L} represent the area-specific capacitance and length-specific capacitance. A is the surface area of the fiber electrode and is equal to π multiplied by the diameter of the fiber electrode (D) and the device active length (L)

$$E = 0.5 C_{\mathrm{A}} V^2 \quad (4)$$

$$P = E/t_{\mathrm{discharge}} \quad (5)$$

The energy density (E) and power density (P) of the GF@PEDOT supercapacitor were obtained from eqn (4) and (5), where V and $t_{\mathrm{discharge}}$ represent the operating voltage and the discharge time.

4. Conclusions

In summary, we successfully fabricated core–shell fibers composed of a GF core with a shell of PEDOT by a facile yet efficient, one-step, hydrothermal strategy combined with an *in situ* interfacial polymerization method. These core–shell structured fibers are flexible and have high conductivity due to the synergistic effects of GFs and PEDOT, respectively. They can be tied into knots and woven into cloth-like structures by hand, thus offering potential electrodes for wearable electronics. We assembled two GF@PEDOT electrodes into a fiber supercapacitor with a specific capacitance of up to 15.39 mF cm^{-2} (0.58 mF cm^{-1}) at 0.53 mA cm^{-2}. This type of fiber supercapacitor will have great potential in the next generation of wearable electronics.

Acknowledgements

This study was supported by the National Natural Science Foundation of China (Grant no: 51602358, 21404124 and 51572303), the High Level Personnel Fund of Zhoukou Normal University (ZKNU2014117), the Program for Innovative Research Team (in Science and Technology) in University of Henan Province (14IRTSTHN009), and the program of Innovative Talent (in Science and Technology) in University of Henan Province (17HASTIT007).

Notes and references

1 X. L. Wang and G. Q. Shi, *Energy Environ. Sci.*, 2015, **8**, 790.
2 X. F. Wang, X. H. Lu, B. Liu, D. Chen, Y. X. Tong and G. Z. Shen, *Adv. Mater.*, 2014, **26**, 4763.
3 W. Weng, P. N. Chen, S. S. He, X. M. Sun and H. S. Peng, *Angew. Chem., Int. Ed.*, 2016, **55**, 2.
4 H. J. Lin, J. Gong, M. Eder, R. Schuetz, H. S. Peng, J. W. C. Dunlop and J. Yuan, *Adv. Mater. Interfaces*, 2017, **4**, 10678.
5 Z. T. Zhang, L. Wang, Y. M. Li, J. Zhang, G. Guan, Z. Pan and H. S. Peng, *Adv. Energy Mater.*, 2017, **7**, 161814.
6 Y. Zhao, Y. Zhang, H. Sun, X. Dong, J. Y. Cao, L. Wang, Y. F. Xu, J. Ren, Y. Hwang, I. H. Son, X. Huang, Y. Wang and H. S. Peng, *Angew. Chem., Int. Ed.*, 2016, **128**, 14596.
7 S. S. He, L. B. Qiu, L. Wang, J. Y. Cao, S. L. Xie, Q. Gao, Z. T. Zhang, J. Zhang, B. J. Wang and H. S. Peng, *J. Mater. Chem. A*, 2016, **4**, 14968.
8 F. Zhao, L. X. Wang, Y. Zhao, L. T. Qu and L. M. Dai, *Adv. Mater.*, 2017, **29**, 1604972.
9 X. P. Wang, J. Gao, Z. H. Cheng, N. Chen and L. T. Qu, *Angew. Chem., Int. Ed.*, 2016, **55**, 14643.
10 H. H. Cheng, F. Zhao, J. L. Xue, G. Q. Shi, L. Jiang and L. T. Qu, *ACS Nano*, 2016, **10**, 9529.
11 F. Xu, Z. W. Tang, S. Q. Huang, L. Y. Chen, Y. R. Liang, W. C. Mai, H. Zhong, R. W. Fu and D. C. Wu, *Nat. Commun.*, 2015, **7**, 7221.
12 W. C. Mai, B. Sun, L. Y. Chen, F. Xu, H. Liu, Y. R. Liang, R. W. Fu, D. C. Wu and K. Matyjaszewski, *J. Am. Chem. Soc.*, 2015, **137**, 13256.
13 F. Xu, H. Xu, X. Chen, D. C. Wu, Y. Wu, H. Liu, C. Gu, R. W. Fu and D. L. Jiang, *Angew. Chem., Int. Ed.*, 2015, **54**, 6814.
14 H. Li, Y. Tao, X. Zheng, J. Y. Luo, F. Y. Kang, H. M. Cheng and Q. H. Yang, *Energy Environ. Sci.*, 2016, **9**, 3135.

15 Y. Xu, Y. Tao, X. Zheng, H. Ma, J. Y. Luo, F. Y. Kang and Q. H. Yang, *Adv. Mater.*, 2015, **27**, 8082.
16 Z. Xu and C. Gao, *Nat. Commun.*, 2011, **2**, 571.
17 Z. L. Dong, C. C. Jiang, H. H. Cheng, Y. Zhao, G. Q. Shi, L. Jiang and L. T. Qu, *Adv. Mater.*, 2012, **24**, 1856.
18 H. P. Cong, X. C. Ren, P. Wang and S. H. Yu, *Sci. Rep.*, 2012, **2**, 613.
19 Y. N. Meng, Y. Zhao, C. G. Hu, H. H. Cheng, Y. Hu, Z. P. Zhang, G. Q. Shi and L. T. Qu, *Adv. Mater.*, 2013, **25**, 2326.
20 Y. Hu, H. H. Cheng, F. Zhao, N. Chen, L. Jiang, Z. H. Feng and L. T. Qu, *Nanoscale*, 2014, **6**, 6448.
21 X. T. Ding, Y. Zhao, C. G. Hu, Y. Hu, Z. L. Dong, N. Chen, Z. P. Zhang and L. T. Qu, *J. Mater. Chem. A*, 2014, **2**, 12355.
22 Q. Chen, Y. N. Meng, C. G. Hu, Y. Zhao, H. B. Shao, N. Chen and L. T. Qu, *J. Power Sources*, 2014, **247**, 32.
23 B. N. Zheng, T. Q. Huang, L. Kou, X. L. Zhao, K. Gopalsamy and C. Gao, *J. Mater. Chem. A*, 2014, **2**, 9736.
24 T. Xu, X. T. Ding, Y. Liang, Y. Zhao, N. Chen and L. T. Qu, *Nanoscale*, 2016, **8**, 12113.
25 G. X. Qu, J. L. Cheng, X. D. Li, D. M. Yuan, P. N. Chen, X. L. Chen, B. Wang and H. S. Peng, *Adv. Mater.*, 2016, **28**, 3646.
26 Y. Liang, Z. Wang, J. Huang, H. H. Cheng, F. Zhao, Y. Hu, L. Jiang and L. T. Qu, *J. Mater. Chem. A*, 2015, **3**, 2547.
27 Y. Wang, *J. Phys.: Conf. Ser.*, 2009, **152**, 012023.
28 L. Jin, T. Wang, Z. Q. Feng, M. K. Leach, J. H. Wu, S. J. Mog and Q. Jiang, *J. Mater. Chem. B*, 2013, **1**, 1818.
29 G. Mariani, Y. Wang, P. S. Wong, A. Lech, C. H. Hung, J. Shapiro, S. Prikhodko, M. El-Kady, R. B. Kaner and D. L. Huffaker, *Nano Lett.*, 2012, **12**, 3581.
30 L. Adamczyk and P. J. Kulesza, *Electrochim. Acta*, 2011, **56**, 3649.
31 P. Matyba, H. Yamaguchi, M. Chhowalla, N. D. Robinson and L. Edman, *ACS Nano*, 2011, **5**, 574.
32 O. Bubnova, Z. U. Khan, A. Malti, S. Braun, M. Fahlman, M. Berggren and X. Crispin, *Nat. Mater.*, 2011, **10**, 429.
33 S. L. McFarlane, B. A. Deore, N. Svenda and M. S. Freund, *Macromolecules*, 2010, **43**, 10241.
34 Z. Q. Feng, J. H. Wu, W. R. Cho, M. K. Leach, E. W. Franz, Y. I. Naim, Z. Z. Gu, J. M. Corey and D. C. Martin, *Polymer*, 2013, **54**, 702.
35 T. P. Nguyen, P. L. Rendu, P. D. Long and S. A. DeVos, *Surf. Coat. Technol.*, 2004, **180–181**, 646.
36 Q. Xu and J. T. Czernuszka, *J. Controlled Release*, 2008, **127**, 146.
37 F. Tran-Van, S. Garreau, G. Louarn, G. Froyer and C. Chevrot, *J. Mater. Chem.*, 2001, **11**, 1378.
38 F. C. Hsu, V. N. Prigodin and A. J. Epstein, *Phys. Rev. B: Condens. Matter Mater. Phys.*, 2006, **74**, 235219.
39 S. Kirchmeyer and K. Reuter, *J. Mater. Chem.*, 2005, **15**, 2077.
40 D. Yu, Q. Qian, L. Wei, W. Jiang, K. Goh, J. Wei, J. Zhang and Y. Chen, *Chem. Soc. Rev.*, 2015, **44**, 647.
41 Y. P. Fu, X. Cai, H. W. Wu, Z. B. Lv, S. C. Hou, M. Peng, X. Yu and D. C. Zou, *Adv. Mater.*, 2012, **42**, 5713.